

A Multiplexed Programmable Quantum Photonic Network

Natalia Herrera Valencia,^{1,*} Annameng Ma,¹ Suraj Goel,¹ Saroch Leedumrongwatthanakun,^{1,†}
Francesco Graffitti,^{1,‡} Alessandro Fedrizzi,¹ Will McCutcheon,¹ and Mehul Malik^{1,§}

¹*Institute of Photonics and Quantum Sciences, Heriot-Watt University, Edinburgh, UK*

Entanglement distribution in quantum networks will enable next-generation technologies for quantum-secured communications, distributed quantum computing and sensing. Future quantum networks will require dense connectivity, allowing multiple parties to share entangled states in a reconfigurable manner, while long-distance connections are established through the teleportation of entangled states, namely entanglement swapping. However, developing flexible physical platforms that can distribute entanglement through a high-capacity and scalable architecture remains a significant challenge. Here we realise a multiplexed programmable network where entanglement is routed and teleported between four parties through a reconfigurable multi-port circuit operating on the transverse-spatial photonic degree-of-freedom. We harness the natural mode-mixing process inside a multi-mode fibre and place it between two programmable phase planes to implement high-dimensional operations for two independent photons carrying eight transverse-spatial modes. This complex-medium-based circuit allows for the control of a four-party state where high-fidelity entangled states can be simultaneously distributed over multiple channels with different on-demand configurations. Our design allows us to break away from the limited planar geometry and bypass the control and fabrication challenges of conventional integrated platforms. Our demonstration showcases the potential of this architecture for enabling quantum networks with scalable and versatile connectivity that is fully compatible with existing communications infrastructure.

Quantum networks enable the distribution and processing of quantum information between distant interconnected quantum nodes, with applications ranging from quantum communication to distributed quantum computing [1]. The distribution of entanglement over multi-user quantum network architectures in an efficient and scalable manner is of paramount importance. In addition to enabling next-generation quantum technologies such as device-independent quantum key distribution [2], entanglement-based networks allow for a distributed configuration that can bolster the performance of quantum computation [3, 4] and quantum metrology [5, 6].

Realising a network where complex entangled states can be shared among multiple remote users requires flexible and high-capacity platforms. Long-distance communication necessitates entanglement swapping [7–9], a form of quantum teleportation where entangling operations between intermediate users facilitate the creation of entanglement between distant users. A multi-user network may also require the flexible routing of bipartite entanglement between different pairs of users within the network [10, 11]. In addition, the network architecture should allow for the multiplexed distribution of quantum information, allowing multiple (qubit) entanglement channels to be simultaneously transmitted over a single link [12]. To realise all these network functionalities in parallel, one needs large, reprogrammable multi-port circuits offering the ability to actively reconfigure the con-

nectivity between users.

State-of-the-art network implementations have demonstrated the flexible routing of bipartite entanglement between multiple users via hybrid multiplexing in bulk and integrated platforms [13–15], as well as the swapping of qubit entanglement between two chips [16]. A recent experiment has even demonstrated the routing of high-dimensional bipartite entanglement between three users over few-mode fibres [17]. However, a network device capable of simultaneously routing and swapping entanglement over multiplexed channels in a reconfigurable manner is yet to be demonstrated. A key challenge is scaling up both the number of modes and photons processed by the device while maintaining circuit fidelity and minimising coupling losses. Conventionally, these circuits are built using the “bottom-up” approach, which relies on a planar mesh arrangement of a large number of carefully controlled interferometers [18]. While impressive circuit dimensionalities of up to 20 modes have been demonstrated recently [19], increasing circuit complexity further will require overcoming many challenges in circuit design and fabrication. Thermal management of the large number of components limits current performance and hinders further scalability [20]. An additional hurdle is presented by the difficulty of efficiently coupling photons from free-space or fibre links into an integrated circuit.

In this context, complex scattering media such as multi-mode fibres (MMFs) have recently emerged as promising candidates for both the transport and manipulation of quantum states of light [21, 22]. Light scattering inside an MMF can be described as a unitary and random linear optical process in a very high-dimensional space. While this effect can be detrimental to the correlations of an entangled state, it can be

* Email address: n.herrera_valencia@hw.ac.uk

† Current address: Division of Physical Science, Faculty of Science, Prince of Songkla University, Songkhla, Thailand

‡ Current address: Cyberhawk, Edinburgh, UK

§ Email address: m.malik@hw.ac.uk; Website: <http://bbqlab.org>

reversed via knowledge of the fibre transmission matrix [23], enabling the transport of high-dimensional spatial entanglement through a complex channel [24]. Using inverse-design techniques, the light scattering process inside the large mode-mixing space of a complex medium can also be harnessed to perform high-dimensional programmable optical circuits by placing the medium (U) between controllable phase planes (P) (see Fig. 1a) [25]. This alternative “top-down” approach simplifies the circuit architecture by separating the control layer from the mixing layer by employing a large number of auxiliary modes, achieving fully programmable high-dimensional quantum gates. Furthermore, it allows one to break out of the restrictive planar geometry of photonic integrated circuits and access the full transverse-spatial photonic degree-of-freedom distributed volumetrically. Finally, using waveguides for both transporting and manipulating quantum states of light steps around the problem of coupling losses between optical links and photonic chips. In recent work, we demonstrated how an MMF-based circuit can be used to manipulate a single photon in its high-dimensional spatial structure, and function as a generalized, programmable multi-outcome measurement device for manipulating and certifying high-dimensional entanglement [25].

Here we build on the top-down approach to realise a MMF-based programmable multi-port device and demonstrate its application in a multiplexed quantum network architecture that allows to route and swap entanglement over multiple channels between four separate users with reconfigurable configurations. Our network architecture is depicted Fig. 1a, overlaid on a map of Scotland as an example scenario. Two independent entanglement sources (circles) generate high-dimensional bipartite entanglement in up to dimension $d = 4$, which is equivalent to two multiplexed qubit-entangled states. A programmable multi-port device (large hexagon) operates on two input photons (s_1 and s_2), enabling the multiplexed distribution of entanglement across four users: Ada (A), Barb (B), Grace (G), and Hedy (H). The ability to reprogram the device operation allows for the adaptable routing of qubit and qutrit entanglement with different network configurations. The entanglement structures shown in Figs. 1b-e illustrate this versatile functionality, where each vertex corresponds to a party, and an edge or link between them represents a shared qubit entangled state. For example, multiplexed qubit entanglement can be shared between user pairs AB and GH (Fig. 1b) or user pairs AG and BH (Fig. 1c). Alternatively, the network can be reconfigured to share qubit entanglement between the four pairs of users AB, AG, HB, and HG. Since the circuit maintains quantum coherence between the input and output modes, it can also be used to implement parallel Bell State measurements on two independent input photons. We can thus teleport entangled states in a multiplexed manner to entangle the two distant users A and H (Fig. 1e).

This implementation showcases the potential of har-

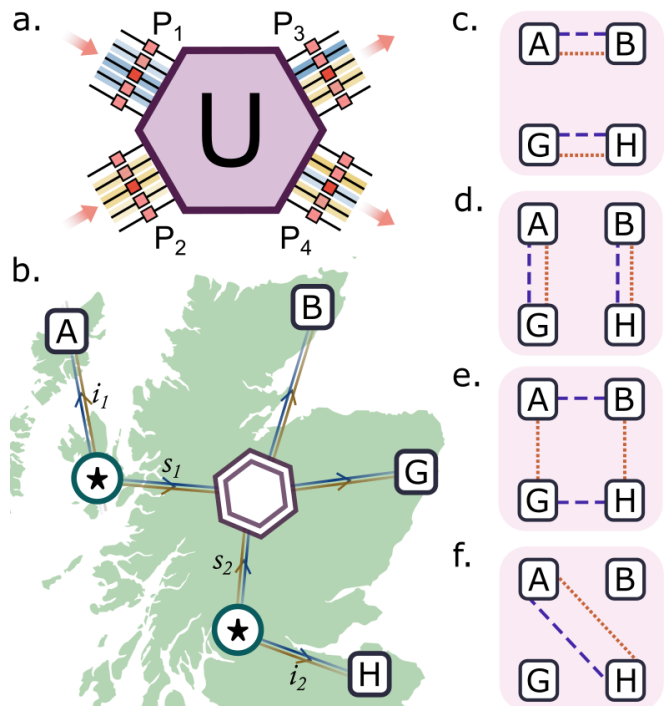


Figure 1. (a) We realise a high-dimensional programmable multi-port device that consists of a complex medium (U) placed between programmable phase planes (P) that allows arbitrary routing and entangling operations on the spatial modes of two input photons. (b) Cartoon depicting an example multiplexed network scenario. Two sources (stars) distribute pairs of high-dimensionally entangled photons to four network users: Ada (A), Barb (B), Grace (G), and Hedy (H). Independent photons (s_1, s_2) from the two sources are injected into the programmable multi-port (hexagon), with outputs directed to users B and G. Their entangled counterparts (i_1, i_2) are sent directly to users A and H. (c-f) The programmable multi-port enables the network architecture to be reconfigured on-demand, allowing us to route and swap multiplexed qubit entanglement between several different configurations of the four users. The blue (dashed) and orange (dotted) lines indicate independent qubit-entanglement channels.

nessing the high-capacity resource of complex-media-based platforms for practical quantum networking. With control of up to eight photonic modes of two independent photons, our multi-port network device manipulates a four-photon state to enable arbitrary and reconfigurable multi-node routing and swapping of entanglement over multiple channels. Furthermore, our fibre-based architecture facilitates coupling to optical links and can maintain a stable operation over days without the need for alignment or recalibration.

I. Programmable Multiport Design

We harness the complexity of the inter-modal coupling inside a random scattering medium to construct

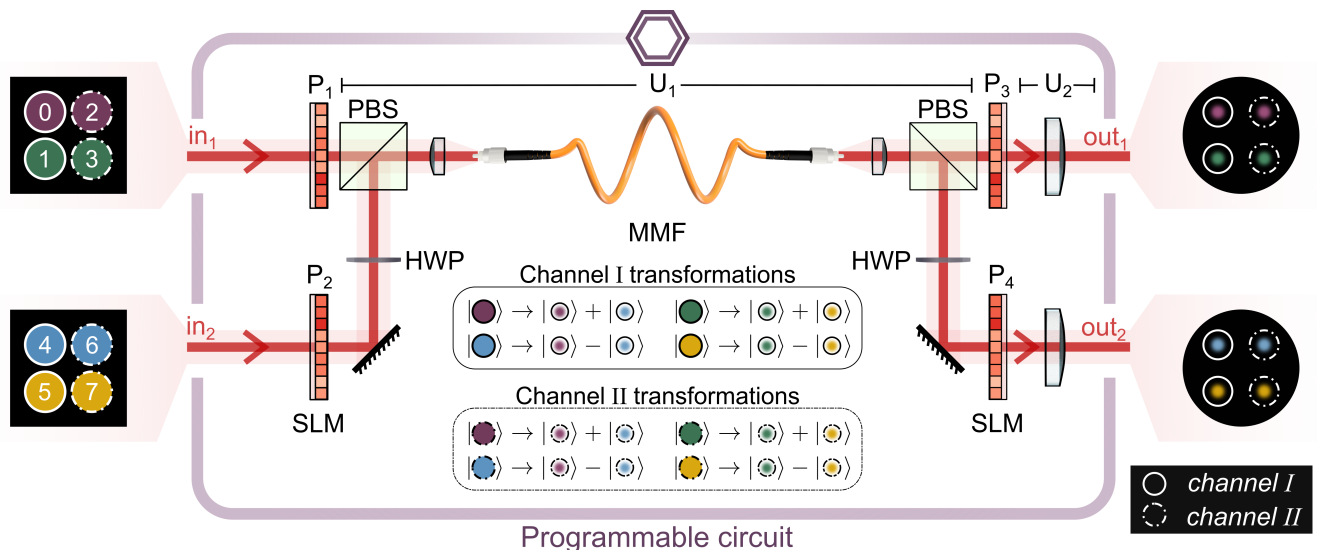


Figure 2. **Complex media-based programmable circuit:** A “top-down” programmable multi-port circuit consisting of a multi-mode fibre (MMF) and two spatial light modulators (SLMs) implementing four phase-planes (P_1 - P_4) manipulates photons from independent spatially entangled pairs injected through in_1, in_2 . The circuit implements transformations of the form $\mathbb{T} = U_2(P_3 + P_4)U_1(P_1 + P_2)$ between input macro-pixel modes (left side) and focused spots across the facet of the MMF (right side), allowing us to route and interfere photonic spatial modes of the two injected photons to manipulate four-photon states over distinct channels. Here we show the transformation between input (in_1, in_2) and output (out_1, out_2) modes for the multiplexed Bell-state measurement that we use to entangle remote parties A and H through two distinct qubit channels. We divide the eight-dimensional sets of input/output modes (labelled 0–7) into two-dimensional subspaces that act as distinct entanglement distribution channels: *channel I* is represented by a solid line and *channel II* by a dash-dotted line. The programmable circuit acts as an 8×8 -dim multi-port beam-splitter in the spatial degree-of-freedom, interfering spatial modes from two independent photons in a multiplexed scheme. PBS: polarising beam splitter, HWP: half-wave plate.

a top-down programmable device that can implement arbitrary high-dimensional two-photon quantum gates. A linear circuit can be represented by a transformation \mathbb{T} that maps a set of input modes to a set of output modes. As depicted in Fig. 2, our design consists of a 30cm-long multi-mode fibre (Thorlabs GIF625), acting as a large ambient mode-mixer, placed between four phase planes displayed on spatial light modulators (SLMs), ensuring the programmability of the platform. The circuit’s transformation can be decomposed as $\mathbb{T} = U_2(P_3 + P_4)U_1(P_1 + P_2)$, with $P_1 - P_4$ representing the reconfigurable phase planes, U_1 describing the transmission through the MMF and associated coupling optics, and U_2 corresponding to the optical system between phase planes P_3/P_4 and the detection system.

The design of the circuit starts with the characterisation of the transformation U_1 across all input modes. We do this measurement using classical illumination and a machine learning model that describes the optical system of the experiment [26]. With complete knowledge of the scattering processes in the mode-mixer, target gates can be inverse-designed using controllable phase pattern solutions for planes P_1/P_4 , displayed on the screens of the programmable SLMs. These patterns are calculated with iterative wavefront matching optimisations of input and output optical fields propagating through all phase planes according to \mathbb{T} [27, 28].

Our multi-port circuit implements high-dimensional quantum operations between modes of discretised transverse position-momentum bases. In the input, we choose the macro-pixel basis [29], composed of localised circular modes as illustrated on the left of Fig. 2. In the output, we target modes randomly selected from a set of focused spots distributed isometrically across the facet of the MMF (Fig. 2, right). To use the full dimensionality of the complex medium platform, we exploit the polarisation dependence in the mode-mixing process of the MMF and associate the two polarisations to two input ports: in_1, in_2 , over which we inject independent photons for coherent control of their spatial modes. At the output, these two polarisations also define the two output ports out_1, out_2 used for directing photons to different users.

Using a four-dimensional macro-pixel modal space $\{|m\rangle\}_m$ with $m = 0, \dots, 3$ for input 1, and $m = 4, \dots, 7$ for input 2, we divide each input set into two separate subspaces. Each two-dimensional modal set is used as a distinct channel for sharing entanglement between network nodes. We define $Ch_I = \{|0\rangle, |1\rangle\}$ and $Ch_{II} = \{|2\rangle, |3\rangle\}$ at input 1, and $Ch_I = \{|4\rangle, |5\rangle\}$ and $Ch_{II} = \{|6\rangle, |7\rangle\}$ at input 2. The same is done with the foci modes at the output to define two different channels at each port.

The circuit enables coherent control over the high-dimensional modal space of two photons from different entangled pairs to distribute entanglement across the

network. Reconfigurable connectivity is implemented by simply targeting different 8×8 unitary operations, without the need for any changes in the setup. For example, we can share entangled states between A-B and G-H with an Identity \mathbb{T}_I gate (Figs 1.c). With a different target operation (\mathbb{T}_X), we can switch the correlations and link A-G and B-H (Figs 1.d.). The circuit also allows for fully connected entanglement configurations like the one in Fig. 1.e through a target \mathbb{T}_M (See explicit definition of the implemented gates in the Supplementary Information S.1). To teleport entanglement and connect distant nodes A and H over two distinct channels (Fig. 1.f), we perform a multiplexed entanglement swapping protocol by targeting the following operation:

$$\mathbb{T}_S = \frac{1}{\sqrt{2}} \begin{bmatrix} 1 & 0 & 0 & 0 & 1 & 0 & 0 & 0 \\ 0 & 1 & 0 & 0 & 0 & 1 & 0 & 0 \\ 0 & 0 & 1 & 0 & 0 & 0 & 1 & 0 \\ 0 & 0 & 0 & 1 & 0 & 0 & 0 & 1 \\ 1 & 0 & 0 & 0 & -1 & 0 & 0 & 0 \\ 0 & 1 & 0 & 0 & 0 & -1 & 0 & 0 \\ 0 & 0 & 1 & 0 & 0 & 0 & -1 & 0 \\ 0 & 0 & 0 & 1 & 0 & 0 & 0 & -1 \end{bmatrix} \quad (1)$$

Implementing this 8-dimensional gate (See the ordering of modes and channels in S.1) allows us to interfere modes from different inputs over individual channels. As illustrated in Fig. 2, the circuit then acts as a multi-port beam-splitter for the four-dimensional macro-pixel basis, enabling a multiplexed Bell-State measurement over the input photons (See S.5 for more details on the entanglement swapping protocol).

II. Reconfigurable Entanglement Network Operation

We demonstrate the operation of the programmable multiport device in a four-user network. Two spontaneous parametric down-conversion (SPDC) sources produce pairs of photons entangled in their position-momentum degrees-of-freedom to distribute over the four users. Each source produces a high-dimensional entangled state on the macro-pixel basis $\{|m\rangle\}_m$: $|\Phi\rangle_1 = \frac{1}{2}(|00\rangle + |11\rangle + |22\rangle + |33\rangle)$ for source 1, and $|\Phi\rangle_2 = \frac{1}{2}(|44\rangle + |55\rangle + |66\rangle + |77\rangle)$ for source 2.

The circuit manipulates the four-party state by injecting photons (s_1 and s_2) from entangled pairs produced by independent sources at the input ports. The other two independent photons (i_1 and i_2) are sent directly to users A and H. Photons exit the circuit through output ports that are directed to users B and G. Each user is equipped with a detection system to perform projective measurements of arbitrary spatial modes using an SLM and coupling to single-mode fibres (SMFs). For a detailed description of the experimental setup, see S.1.

Table I: Fidelities [%] to the maximally entangled state of the states shared in the multiplexed programmable network using 8-dimensional gates

\mathbb{T}_I	AB 1	AB 2	GH 1	GH 2
	86.0 ± 1.0	78.6 ± 0.9	86.3 ± 0.9	79.2 ± 1.1
\mathbb{T}_X	AG 1	AG 2	BH 1	BH 2
	81.6 ± 1.0	79.2 ± 1.1	81.7 ± 1.2	80.8 ± 1.1
\mathbb{T}_M	AB 1	AG 2	BH 1	GH 2
	82.3 ± 1.0	81.2 ± 1.2	76.5 ± 1.2	81.4 ± 1.0
\mathbb{T}_S	AH 1		AH 2	
	77.1 ± 3.3		83.2 ± 2.7	

*Errors are reported to a standard deviation

To characterise the functionality of the adaptable entanglement routing, we use two-fold coincidences between the four parties to measure correlations for each multiplexed network configuration. The implementation of gate \mathbb{T}_I is illustrated in Fig. 3.a, where measurements in two mutually unbiased bases show correlations between A-B and G-H over the four modes composing Channel I and Channel II. In the same manner, multiplexed correlations between A-G and B-H are observed with the implementation of the target gate operation \mathbb{T}_X Fig. 3.b. A fully connected network is achieved by implementing \mathbb{T}_M , where each user is correlated to the other two users over different two-dimensional modal subspaces (3.c).

We take correlation measurements over the three mutually unbiased bases of each two-dimensional modal subspace or channel and use a fidelity witness [30] to certify the multiplexed entanglement distribution in all network configurations. As shown in Table. I, we estimate the fidelities of all the states shared in the network to the two-dimensional maximally entangled state. With the implementation of \mathbb{T}_I , state fidelities above 79% demonstrate the distribution of qubit entangled states over two channels between users A and B, and users G and H. In the same manner, the fidelities of the states shared through gate \mathbb{T}_X demonstrate qubit entanglement over two distinct channels between A-G and B-H. The distribution of entanglement between the four pairs of users AB, AG, BH, and GH with \mathbb{T}_M is demonstrated with fidelities above 76%. Errors in the fidelities are calculated using a Monte Carlo simulation that takes into account photon statistics.

Additionally, we test the stability of the programmable circuit over time (see S.4) by repeatedly implementing all 8×8 gate operations and measuring the fidelity to the maximally entangled state of all distributed states over 14 days. Maintaining the position and bending of the multi-mode fibre with simple coupling stages or clamps to the optical table, the fidelity of the entangled states remains well above the bound, without the need for re-

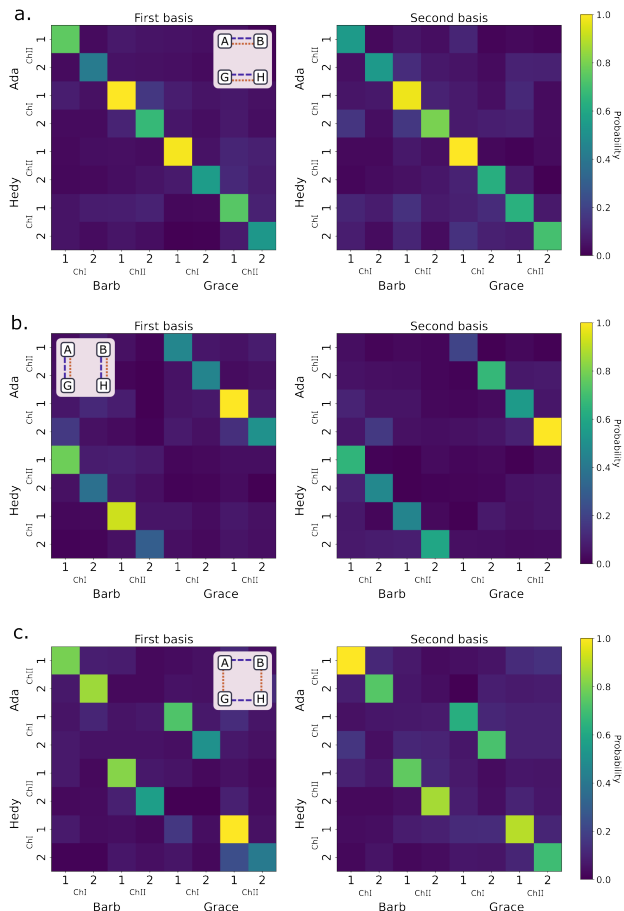


Figure 3. **Multiplexed entanglement routing.** We target 8-dimensional unitary operations to distribute two-dimensional entanglement over two distinct channels with different configurations (insets). Using different modal subspaces as distribution channels, each user in the network can simultaneously share two entangled states, either with one other user (a,b) or with two other users (c). We perform measurements on mutually unbiased bases to characterise the operation of each configuration. The correlation matrices correspond to two-fold coincidence measurements on the first (left) and second (right) bases, showcasing the circuit’s operation.

alignment or re-characterisation of the mode-mixing process, demonstrating the robustness of the multi-port device.

In the case of the multiplexed entanglement swapping protocol, four-fold measurements over the network users allow us to characterise the resulting state between distant parties Ada (A) and Hedy (H) through quantum state tomography (Details on the state estimation are given in S.6). As shown in Fig 4, we recover the density matrices of the two states shared by A and H. The estimated states on each channel have fidelities to a two-dimensional maximally entangled target state of the form $|\Psi_T\rangle = \frac{1}{\sqrt{2}}(|0_A 1_H\rangle - e^{i\theta}|1_A 0_H\rangle)$ of more than 77% (with the phase $\theta = 1.535\pi$ arising from the relative phase be-

tween input polarisations), demonstrating the success of the entanglement swapping protocol.

We can also harness the high dimensionality of the entanglement produced by the SPDC sources to distribute high-dimensional entanglement with different on-demand configurations. As shown in S.3, measurements in mutually unbiased bases allow us to certify three-dimensional entangled states between AB and GH (Identity gate), or AG and BH (Switch gate).

We note that due to our users’ detection devices containing only one SNSPD each, we perform the tomography/witnesses for each state/channel separately, whereas equipping each use with multiple detectors would enable their multiplexed states to be recorded simultaneously/in parallel, with no reconfiguring of the programmable circuit.

III. Conclusion and Outlook

We have implemented a programmable photonic network that harnesses the large mode-mixing process inside a multi-mode fibre to distribute and teleport entanglement between four users over multiple channels. Our reconfigurable MMF-based circuit enables flexible network connectivity, where entanglement can be shared between the users in different on-demand configurations, without any changes to the experimental setup. Using this device, We demonstrate control over a four-photon state through operations on two independent photons in up to eight photonic modes, achieving multiplexed routing and swapping of qubit entanglement with fidelities to the maximally entangled state of above 76% for all network configurations and channels. We also demonstrate the routing of qutrit entanglement, showcasing the versatility our MMF-based device. To enable a multiplexed operation, two-dimensional spatial-mode subspaces are used as distinct entanglement distribution channels, allowing users to share multiple qubit-entangled states simultaneously. Moreover, our ability to perform programmable Bell-state measurements on different spatial-mode subspaces enables us to link two remote users through simultaneous entanglement swapping over two different channels.

Our multi-port device allows for efficient integration into existing communications infrastructure because of its straightforward coupling to optical fibre links. The stability of our system is maintained over weeks, and there is no need for special protective enclosures or recalibration of the mode-mixing process. With our top-down approach, the fidelity and size of the operations can be improved with a higher number of programmable phase layers within the circuit or a larger dimensionality in the auxiliary modal space offered by the MMF [25]. However, effects such as loss or modal dispersion become more prevalent in these regimes, and shorter fibre lengths or spectral-temporal control techniques may be necessary. Nevertheless, our device serves as a power-

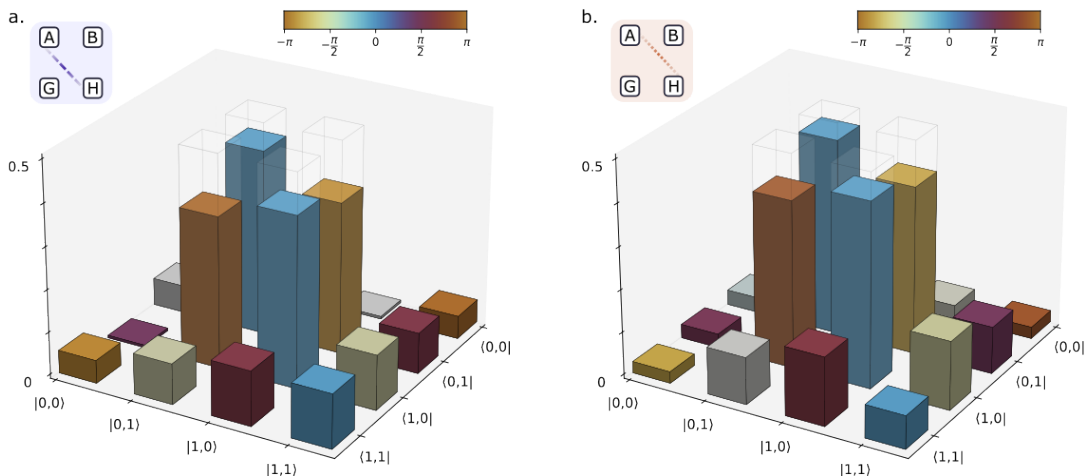


Figure 4. **Multiplexed entanglement swapping:** We perform quantum state tomography to estimate the states shared between Ada and Hedy after the multiplexed SWAP operation. We obtain fidelities to the two-dimensional maximally entangled target states $|\Psi_T\rangle$ (transparent bars, with $\theta = 1.535\pi$) of $77.1 \pm 9.8\%$ for the first channel, and $83.2 \pm 8.3\%$ for the second one, demonstrating the success of our entanglement swapping protocol.

ful alternative for multi-node, multi-mode entanglement distribution over a network with reconfigurable connectivity. As the number of modes is increased, the characterisation of such a device may require efficient process fidelity witnesses based on minimal measurements [31]. Future implementations of such a multi-port device could also explore entanglement in different high-dimensional spatial-mode bases [32], and other photonic degree-of-freedom such as time-energy [33]. Our imple-

mentation demonstrates the potential of complex-media-based platforms for realizing practical and noise-robust quantum network architectures [34] and the control and distribution of large quantum photonic states.

Acknowledgements: We acknowledge financial support from the UK Engineering and Physical Sciences Research Council (EPSRC) (EP/P024114/1), European Research Council (ERC) Starting Grant PIQUANT (950402), and the Royal Academy of Engineering Chair in Emerging Technologies programme (CiET-2223-112).

-
- [1] H. Kimble, *The quantum internet*, *Nature* **453**, 1023 (2008), arXiv:0806.4195v1.
- [2] Umesh Vazirani and Thomas Vidick, *Fully device-independent quantum key distribution*, *Phys. Rev. Lett.* **113**, 140501 (2014), arXiv:1210.1810v2.
- [3] J. I. Cirac, A. K. Ekert, S. F. Huelga, and C. Macchiavello, *Distributed quantum computation over noisy channels*, *Physical Review A* **59**, 4249 (1999), arXiv:quant-ph/9803017.
- [4] J. Eisert, K. Jacobs, P. Papadopoulos, and M. B. Plenio, *Optimal local implementation of nonlocal quantum gates*, *Physical Review A* **62**, 052317 (2000), arXiv:quant-ph/0005101.
- [5] P. Kómár, E. M. Kessler, M. Bishof, L. Jiang, A. S. Sørensen, J. Ye, and M. D. Lukin, *A quantum network of clocks*, *Nature Physics* **10**, 582 (2014), arXiv:1310.6045.
- [6] Xueshi Guo, Casper R. Breum, Johannes Borregaard, Shuro Izumi, Mikkel V. Larsen, Tobias Gehring, Matthias Christandl, Jonas S. Neergaard-Nielsen, and Ulrik L. Andersen, *Distributed quantum sensing in a continuous-variable entangled network*, *Nature Physics* **16**, 281 (2019), arXiv:1905.09408.
- [7] M. Zukowski, A. Zeilinger, M. A. Horne, and A. K. Ekert, *“event-ready-detectors” bell experiment via entanglement swapping*, *Physical Review Letters* **71**, 4287 (1993).
- [8] Jian-Wei Pan, Dik Bouwmeester, Harald Weinfurter, and Anton Zeilinger, *Experimental entanglement swapping: Entangling photons that never interacted*, *Phys. Rev. Lett.* **80**, 3891 (1998).
- [9] M. Pompili, S. L.N. Hermans, S. Baier, H. K.C. Beukers, P. C. Humphreys, R. N. Schouten, R. F.L. Vermeulen, M. J. Tiggelman, L. dos Santos Martins, B. Dirkse, S. Wehner, and R. Hanson, *Realization of a multi-mode quantum network of remote solid-state qubits*, *Science* **372**, 259 (2021), arXiv:2102.04471.
- [10] Manuel Erhard, Mehul Malik, and Anton Zeilinger, *A quantum router for high-dimensional entanglement*, *Quantum Science and Technology* **2**, 014001 (2017), arXiv:1605.05947.
- [11] I. Herbauts, T. Jennewein, A. Poppe, H. Hübel, and B. Blauensteiner, *Demonstration of active routing of entanglement in a multi-user network*, *Optics Express* **21**, 29013 (2013), arXiv:1307.5462.
- [12] Sören Wengerowsky, Siddarth Koduru Joshi, Fabian Steinlechner, Hannes Hübel, and Rupert Ursin, *An entanglement-based wavelength-multiplexed quantum communication network*, *Nature* **564**, 225 (2018), arXiv:1801.06194.
- [13] Siddarth Koduru Joshi, Djeylan Aktas, Sören

- Wengerowsky, Martin Lončarić, Sebastian Philipp Neumann, Bo Liu, Thomas Scheidl, Guillermo Currás Lorenzo, Željko Samec, Laurent Kling, Alex Qiu, Mohsen Razavi, Mario Stipčević, John G. Rarity, and Rupert Ursin, *A trusted node-free eight-user metropolitan quantum communication network*, *Science Advances* **6** (2020), arXiv:1907.08229.
- [14] Félicien Appas, Florent Baboux, Maria I. Amanti, Aristide Lemaitre, Fabien Boitier, Eleni Diamanti, and Sara Ducci, *Flexible entanglement-distribution network with an algaas chip for secure communications*, *npj Quantum Information* **7**, 1 (2021), arXiv:2102.04835.
- [15] Muneer Alshowkan, Philip G. Evans, Brian P. Williams, Nageswara S.V. Rao, Claire E. Marvinney, Yun Yi Pai, Benjamin J. Lawrie, Nicholas A. Peters, and Joseph M. Lukens, *Advanced architectures for high-performance quantum networking*, *Journal of Optical Communications and Networking* **14**, 493 (2022), arXiv:2111.15547.
- [16] Daniel Llewellyn, Yunhong Ding, Imad I. Faruque, Stefano Paesani, Davide Bacco, Raffaele Santagati, Yan Jun Qian, Yan Li, Yun Feng Xiao, Marcus Huber, Mehul Malik, Gary F. Sinclair, Xiaoqi Zhou, Karsten Rottwitt, Jeremy L. O'Brien, John G. Rarity, Qihuang Gong, Leif K. Oxenlowe, Jianwei Wang, and Mark G. Thompson, *Chip-to-chip quantum teleportation and multi-photon entanglement in silicon*, *Nature Physics* **16**, 148 (2019).
- [17] Yun Zheng, Chonghao Zhai, Dajian Liu, Jun Mao, Xiaojiong Chen, Tianxiang Dai, Jieshan Huang, Jueming Bao, Zhaorong Fu, Yeyu Tong, Xuotong Zhou, Yan Yang, Bo Tang, Zhihua Li, Yan Li, Qihuang Gong, Hon Ki Tsang, Daoxin Dai, and Jianwei Wang, *Multichip multidimensional quantum networks with entanglement retrievability*, *Science* **381**, 221 (2023).
- [18] William R. Clements, Peter C. Humphreys, Benjamin J. Metcalf, W. Steven Kolthammer, Ian A. Walmsley, and Ian A. Walmsley, *Optimal design for universal multipoint interferometers*, *Optica* **3**, 1460 (2016), arXiv:1603.08788.
- [19] Caterina Taballione, Malaquias Correa Anguita, Michiel de Goede, Pim Venderbosch, Ben Kassenberg, Henk Snijders, Narasimhan Kannan, Ward L. Vleeshouwers, Devin Smith, Jörn P. Epping, Reinier van der Meer, Pepijn W.H. Pinkse, Hans van den Vlekert, and Jelmer J. Renema, *20-mode universal quantum photonic processor*, *Quantum* **7**, 1071 (2023).
- [20] Shusmitha Kyatam, Joana C. Mendes, Hugo Neto, and Debarati Mukherjee, *Thermal management of photonic integrated circuits: impact of holder material and epoxies*, *Applied Optics* **58**, 6126 (2019).
- [21] Hugo Defienne, Marco Barbieri, Ian A Walmsley, Brian J Smith, and Sylvain Gigan, *Two-photon quantum walk in a multimode fiber*, *Sci. Adv.* **2**, e1501054 (2015), arXiv:1504.03178.
- [22] Saroch Leedumrongwattanakun, Luca Innocenti, Hugo Defienne, Thomas Juffmann, Alessandro Ferraro, Mauro Paternostro, and Sylvain Gigan, *Programmable linear quantum networks with a multimode fibre*, *Nature Photonics* **14**, 139 (2020), arXiv:1902.10678.
- [23] S M Popoff, G Lerosey, R Carminati, M Fink, A C Boccara, and S Gigan, *Measuring the transmission matrix in optics: An approach to the study and control of light propagation in disordered media*, *Phys. Rev. Lett.* **104**, 100601 (2010).
- [24] Natalia Herrera Valencia, Suraj Goel, Will McCutcheon, Hugo Defienne, and Mehul Malik, *Unscrambling entanglement through a complex medium*, *Nature Physics* **16**, 1112 (2020), arXiv:1910.04490.
- [25] Suraj Goel, Saroch Leedumrongwattanakun, Natalia Herrera Valencia, Will McCutcheon, Armin Tavakoli, Claudio Conti, Pepijn W. H. Pinkse, and Mehul Malik, *Inverse-design of high-dimensional quantum optical circuits in a complex medium*, *Nature Physics* **16**, 232 (2024), arXiv:2204.00578.
- [26] Suraj Goel, Claudio Conti, Saroch Leedumrongwattanakun, and Mehul Malik, *Referenceless characterization of complex media using physics-informed neural networks*, *Opt. Express* **31**, 32824 (2023), arXiv:2303.16041.
- [27] M. Kohtoku, I. Ogawa, T. Shibata, T. Saida, H. Takahashi, and T. Hashimoto, *Optical circuit design based on a wavefront-matching method*, *Optics Letters* **30**, 2620 (2005).
- [28] Toshikazu Hashimoto, Takashi Saida, Yohei Sakamaki, and Hiroshi Takahashi, *New optical waveguide design based on wavefront matching method*, *Journal of Lightwave Technology* **25**, 3511 (2007).
- [29] Natalia Herrera Valencia, Vatshal Srivastav, Matej Pivoluska, Marcus Huber, Nicolai Friis, Will McCutcheon, and Mehul Malik, *High-Dimensional Pixel Entanglement: Efficient Generation and Certification*, *Quantum* **4**, 376 (2020), arxiv:2004.04994.
- [30] Jessica Bavaresco, Natalia Herrera Valencia, Claude Klöckl, Matej Pivoluska, Paul Erker, Nicolai Friis, Mehul Malik, and Marcus Huber, *Measurements in two bases are sufficient for certifying high-dimensional entanglement*, *Nature Physics* **14**, 1032 (2017), arXiv:1709.07344.
- [31] Sophie Engineer, Suraj Goel, Sophie Egelhaaf, Will McCutcheon, Vatshal Srivastav, Saroch Leedumrongwattanakun, Sabine Wollmann, Ben Jones, Thomas Cope, Nicolas Brunner, Roope Uola, and Mehul Malik, *Certifying high-dimensional quantum channels*, arXiv (2024), arXiv:2408.15880.
- [32] Mehul Malik and Robert W Boyd, *Quantum imaging technologies*, *Rivista Del Nuovo Cimento* **37**, 273 (2014).
- [33] Anand Kumar Jha, Mehul Malik, and Robert W Boyd, *Exploring energy-time entanglement using geometric phase*, *Physical Review Letters* **101**, 180405 (2008).
- [34] Vatshal Srivastav, Natalia Herrera Valencia, Will McCutcheon, Saroch Leedumrongwattanakun, Sébastien Designolle, Roope Uola, Nicolas Brunner, and Mehul Malik, *Quick quantum steering: Overcoming loss and noise with qudits*, *Physical Review X* **12**, 041023 (2022).
- [35] Vatshal Srivastav, Natalia Herrera Valencia, Saroch Leedumrongwattanakun, Will McCutcheon, and Mehul Malik, *Characterizing and tailoring spatial correlations in multimode parametric down-conversion*, *Physical Review Applied* **18**, 054006 (2022), arxiv:2110.03462.
- [36] C. K. Law and J. H. Eberly, *Analysis and interpretation of high transverse entanglement in optical parametric down conversion*, *Physical Review Letters* **92**, 127903 (2004).
- [37] Francesco Graffitti, Jérémy Kelly-Massicotte, Alessandro Fedrizzi, and Agata M. Brańczyk, *Design considerations for high-purity heralded single-photon sources*, *Physical Review A* **98**, 053811 (2018).
- [38] Francesco Graffitti, Peter Barrow, Massimiliano Proietti, Dmytro Kundys, and Alessandro Fedrizzi, *Independent*

- high-purity photons created in domain-engineered crystals*, *Optica* **5**, 514 (2018), [arXiv:1712.07140](#).
- [39] Daria Andreoli, Giorgio Volpe, Sébastien Popoff, Ori Katz, Samuel Grésillon, and Sylvain Gigan, *Deterministic control of broadband light through a multiply scattering medium via the multispectral transmission matrix*, *Scientific Reports* **5** (2015), [arXiv:1412.0368](#).
- [40] Joel Carpenter, Benjamin J. Eggleton, and Jochen Schröder, *Complete spatiotemporal characterization and optical transfer matrix inversion of a 420 mode fiber*, *Optics Letters* **41**, 5580 (2016).
- [41] Wen Xiong, Chia Wei Hsu, Yaron Bromberg, Jose Enrique Antonio-Lopez, Rodrigo Amezcua Correa, and Hui Cao, *Complete polarization control in multimode fibers with polarization and mode coupling*, *Light: Science & Applications* **7**, 1 (2018), [arXiv:1709.01029](#).
- [42] Zdeněk Hradil, Jaroslav Řeháček, Jaromír Fiurášek, and Miroslav Ježek, *3 maximum-likelihood methods in quantum mechanics*, in *Quantum State Estimation*, edited by Matteo Paris and Jaroslav Řeháček (Springer Berlin Heidelberg, Berlin, Heidelberg, 2004) pp. 59–112.

Supplementary information for: A Multiplexed Programmable Quantum Photonic Network

The following supplementary information is provided: Details of the experimental setup (S.1), techniques for characterising the complex scattering in the multi-mode fibre and designing optical circuits (S.2), results for two and three-dimensional entanglement routing over a single channel (S.3), performance of the circuit over time (S.4), single and two-channel entanglement swapping (S.5), and method for estimating the swapped states through quantum state tomography (S.6).

S.1. Detailed experimental setup

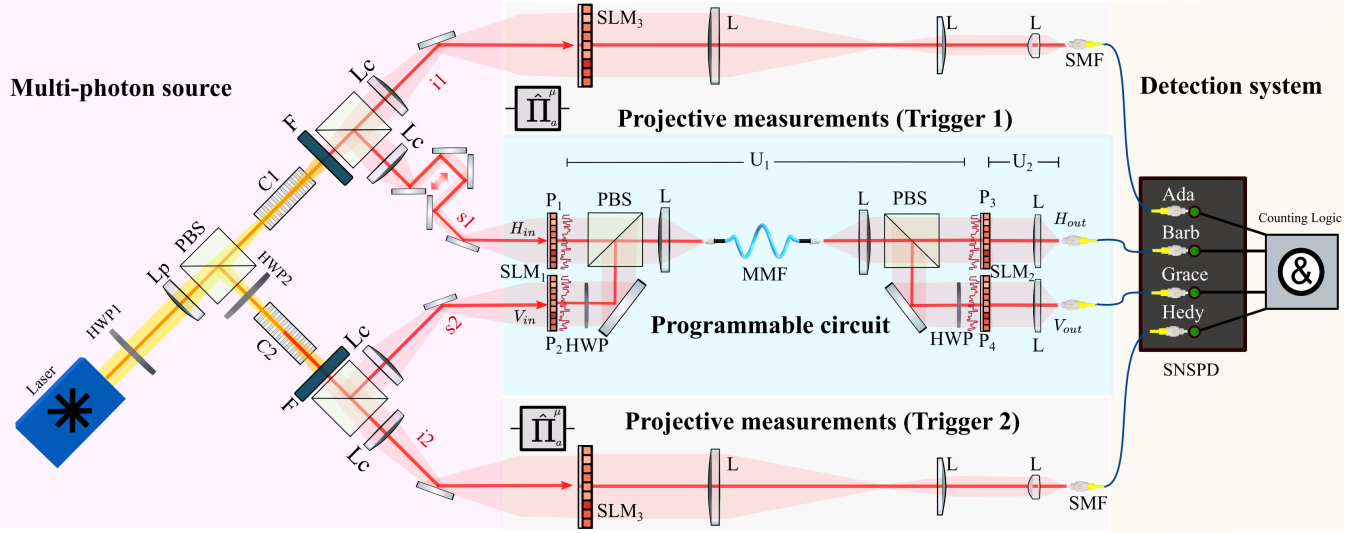


Figure S.1. **Experimental implementation** Two pairs of high-dimensional spatially entangled states are generated through spontaneous parametric down-conversion in periodically poled Potassium Titanyl Phosphate (ppKTP) crystals (C1 and C2). The signal photons of each pair (s_1 and s_2) are sent towards Barb or Grace through the programmable circuit composed of a multi-mode optical fibre (MMF) and two spatial light modulators (SLM₁ and SLM₂). To ensure both input photons are indistinguishable through the circuit, identical paths are ensured with a delay stage on the path of s_1 . Users Barb and Grace use SLM₂ to scan over different output modes. The other two photons of each entangled state (i_1 and i_2) are sent directly to users Alice and Hedy, who perform projective measurements in spatial modes by combining a spatial light modulator (SLM₃) and a single-mode fibre (SMF). Notice that the screen on each SLM is divided into two sections, each for manipulating a different photon. The photons of each user are coupled to SMFs that guide them to superconducting nanowire single-photon detectors (SNSPD). Coincidence events between the four parties are registered through a time-tagging counting logic. The network can implement different high-dimensional gates, allowing Ada, Barb, Grace and Hedy to share entangled states with multiple configurations. L: lens, PBS: polarised beam-splitter, F: filter

The experimental setup for our programmable network is illustrated in S.1. The setup can be divided into three sections:

- **Entangled photon sources:** A 4-photon state composed of two independent pairs of photons generated through Type II SPDC at 1550 nm in two identical non-linear periodically poled Potassium Titanyl Phosphate (ppKTP) crystals (1 mm×2 mm×5 mm).
- **Programmable circuit:** Using a “top-down” approach, a 30 cm-long graded-index fibre (Thorlabs GIF625) acting as a complex mode-mixer, and supporting approximately 150 modes per polarisation at 1550 nm, is placed between two programmable phase layers each comprising of two phase planes ($\{P_1, P_2\}$ and $\{P_3, P_4\}$) implemented on two spatial-light-modulators (Hamamatsu X10468-08).
- **Detection system:** Single-outcome projections on photons exiting the circuit, as well as on the pair of photons used as heralding triggers, are executed with the combination of spatial light modulators, coupling to single-mode-fibres and superconducting nanowire detectors. On the other side, classical light propagating through the circuit is measured with an InGaAs camera (Allied Vision, Goldeye G-008 Cool TEC1) to characterise the complex mode-mixing in the fibre and initial testing of the gates.

S.1.1. Multi-photon source

A 775-nm Ti:Sapphire femtosecond pulsed laser (140fs) is divided into two beams with a polarised beam-splitter (PBS) and a half-wave plate (HWP1). Each beam is focused with a power of 750 mW onto each ppKTP crystal (1mm \times 2mm \times 5mm) to generate independent pairs of entangled photons. With a lens L_p ($f_p = 150$ mm) we set the beam waist ($1/e^2$ radius) of the pump at the centre of each crystal to $w_p = 62\mu\text{m}$. With this waist, we estimate a Schmidt number of each of the generated biphoton states of $K_G \sim 6$ [35, 36]. Since the collection optics will further reduce the available entanglement, this modal bandwidth is an upper bound of the dimensionality we expect from each entangled pair.

The energy- and phase-matching conditions for these pump and crystal parameters lead to some non-separability in the joint-spectral amplitude (JSA), thus reducing heralded single-photon purity. This limits the Hong-Ou-Mandel interference visibility and the subsequent entanglement swapping fidelity. This reasoning is more nuanced when considering multiple spatial modes, whose JSAs may be distinct. However, our configuration minimises the spatial-spectral coupling across the spatial modes of interest [35] so the JSAs should be well approximated by the collinear JSA. A natural route to improving this purity would be to reduce the spectral bandwidth of the pump, decrease the crystal length, or introduce spectral bandpass filters on the photon(s) [37]. Domain-engineered crystals could also be employed to tailor the crystal nonlinearity, eliminating the need for narrowband spectral filtering. This would reduce losses while improving the overall signal-to-noise ratio [38]

An alternative route to spectral filtering originates from the finite spectral bandwidth of the scattering medium [39, 40]. Since the operations programmed in the MMF are optimised for the central wavelength at which it was classically characterised, the reduced mode transformation efficiency at more distant frequencies leads to effective spectral filtering into the desired output mode. This effect was sufficient to observe approximately 10 nm Gaussian spectral filtering on our programmed identity gate, allowing us to obtain high-quality swapped state fidelities even after the removal of spectral bandpass filters used for the classical characterisation. The precise nature of these effects depends intimately on the spatial modes in use, gate transformation implemented, the dispersive properties of the random configuration of the MMF, as well as the spectral-spatial properties of the bi-photon state generated in the crystal, as such, the contributions to our swapped state fidelities cannot be exactly isolated.

After the crystal, the pump is dumped using a dichroic mirror (corresponding to filter F in the figure), and the signal and idler photons of each source are separated using a PBS. The signal photons s_1 and s_2 are injected into the optical circuit with orthogonal polarisations (more details in the following section). To control their indistinguishability, we introduced a temporal delay with a motorised stage on the path of s_1 . The idler photons i_1 and i_2 are manipulated with an SLM and SMF combination, allowing for single outcome projective measurements in arbitrary spatial modes. Taking into account the physical parameters of the SPDC generation, we estimate the correlation bandwidth σ_S of the biphoton states at the Fourier plane and use a set of three lenses between crystal and SLMs to adequately collect and resize the pair of photons such that they cover most of the area of each SLM screen (600 \times 400 pixels with 20 μm pixel pitch), but avoids any clipping. For the sake of simplicity, this optical system is represented in S.1 by the lens L_c . After reflection from SLMs, a telescope system and an aspheric lens are used for mode-matching the projected photons to either SMF or MMF collection modes (In S.1, this optical system is labeled as L inside the programmable circuit section, and shown explicitly with the three lenses in the projective measurements section).

S.1.2. Programmable optical circuit

A “top-down” programmable optical circuit [25] harnesses random scattering inside a multi-mode fibre. The circuit is designed to operate on the macro-pixel basis on the input side, while the target output modes are randomly selected from the set of all possible focused spots (foci) distributed isometrically across the facets of the MMF. Note that our fibre only supports approximately 150 spatial modes per polarisation, but we over-sample the facet of the fibre to improve the characterisation of the transmission matrix.

The mode-mixing process inside the fibre is dependent on polarisation. Light with horizontal polarisation has a different transmission matrix than light with vertical polarisation. Furthermore, modes with a given polarisation will exit the fibre in two different polarisations because polarisation isn’t preserved. This polarisation mixing allows us to take advantage of the full modal space offered by the multi-mode fibre by defining the ports of the circuit according to polarisation [22, 41]. As shown in S.1, we have two input photon ports (Input 1 is H_{in} and Input 2 is V_{in}) and two output photon ports (Output 1 is H_{out} , and Output 2 is V_{out}).

The screen of SLM₁ is divided into two regions to be used as phase planes P_1 and P_2 , allowing for the independent control of light entering from each input port. While the signal photons (s_1 and s_2) are generated with the same polarisation in their respective crystal, we rotate the polarisation of one of the photons (not shown in the figure), superposed them with a polarised beam splitter (PBS), and inject them into the MMF with orthogonal polarisations.

Light coming out of the fibre is separated using a second PBS, with each output polarisation reflecting on a different region of SLM2 to be used as phase planes P_3 and P_4 , and directed to its corresponding detection stage.

We implement four different kinds of circuits defined by operations $\{\mathbb{T}_I, \mathbb{T}_X, \mathbb{T}_M, \mathbb{T}_S\}$, with:

$$\mathbb{T}_I = \begin{bmatrix} 1 & 0 & 0 & 0 & 0 & 0 & 0 & 0 \\ 0 & 1 & 0 & 0 & 0 & 0 & 0 & 0 \\ 0 & 0 & 1 & 0 & 0 & 0 & 0 & 0 \\ 0 & 0 & 0 & 1 & 0 & 0 & 0 & 0 \\ 0 & 0 & 0 & 0 & 1 & 0 & 0 & 0 \\ 0 & 0 & 0 & 0 & 0 & 1 & 0 & 0 \\ 0 & 0 & 0 & 0 & 0 & 0 & 1 & 0 \\ 0 & 0 & 0 & 0 & 0 & 0 & 0 & 1 \end{bmatrix}, \quad \mathbb{T}_X = \frac{1}{\sqrt{2}} \begin{bmatrix} 0 & 0 & 0 & 0 & 1 & 0 & 0 & 0 \\ 0 & 0 & 0 & 0 & 0 & 1 & 0 & 0 \\ 0 & 0 & 0 & 0 & 0 & 0 & 1 & 0 \\ 0 & 0 & 0 & 0 & 0 & 0 & 0 & 1 \\ 1 & 0 & 0 & 0 & 0 & 0 & 0 & 0 \\ 0 & 1 & 0 & 0 & 0 & 0 & 0 & 0 \\ 0 & 0 & 1 & 0 & 0 & 0 & 0 & 0 \\ 0 & 0 & 0 & 1 & 0 & 0 & 0 & 0 \end{bmatrix}, \quad \mathbb{T}_M = \frac{1}{\sqrt{2}} \begin{bmatrix} 1 & 0 & 0 & 0 & 0 & 0 & 0 & 0 \\ 0 & 1 & 0 & 0 & 0 & 0 & 0 & 0 \\ 0 & 0 & 0 & 0 & 1 & 0 & 0 & 0 \\ 0 & 0 & 0 & 0 & 0 & 1 & 0 & 0 \\ 0 & 0 & 1 & 0 & 0 & 0 & 0 & 0 \\ 0 & 0 & 0 & 1 & 0 & 0 & 0 & 0 \\ 0 & 0 & 0 & 0 & 0 & 0 & 1 & 0 \\ 0 & 0 & 0 & 0 & 0 & 0 & 0 & 1 \end{bmatrix}, \quad (\text{S.1.1})$$

The operation for the multiplexed entanglement swapping protocol \mathbb{T}_S is defined in Eq.1 of the main text. Labels indicating the ordering of modes and channels are shown in Table S.1.

			In1		In2						
			Ch I	Ch II	Ch I	Ch II					
Channels		Modes	0	1	2	3	4	5	6	7	
		Out 1	Ch I	0	1	0	0	0	1	0	0
1	0			1	0	0	0	0	1	0	
Ch II	2		0	0	1	0	0	0	0	1	0
	3		0	0	0	1	0	0	0	0	1
Out 2	Ch I	4	1	0	0	0	-1	0	0	0	
		5	0	1	0	0	0	0	-1	0	
	Ch II	6	0	0	1	0	0	0	0	-1	0
		7	0	0	0	1	0	0	0	0	-1

Table S.1. Transformation between input and output modes over two channels implemented with operation \mathbb{T}_S .

S.1.3. User node: Detection and state analysis

Projective spatial measurements on idler photons. $\hat{\Pi}_a^\mu$ in any spatial mode a of basis μ , are performed using SLM₃ and coupling to SMFs, which guide the photons to parties A and H.

For the pair of photons going through the circuit, SLM₂ is used to display the wavefront matching solution of the targeted operation, while simultaneously projecting the light from the two selected outputs ports to couple to SMFs that are guided towards users B and G.

The collected photons from the heralding side and the output ports of the circuit are sent to superconducting nanowire single-photon detectors (Quantum Opus, Opus One, efficiency >85% at 1550 nm). A counting logic (Swabian, TimeTagger Ultra) records coincidences between the 4 channels with a window of 200 ps.

When sending light from a classical source through the system, a removable mirror allows us to switch, without introducing changes in the circuit, from single-photon detection to imaging of the output speckle patterns using an InGaAs camera. A 400 mm lens focuses light reflecting from the SLM onto the sensor of the camera, where images of the output facet of the fibre are taken for the characterisation of U_2 and the initial test of the circuit's functionality.

S.2. Characterization of complex mode-mixer and inverse design of optical circuit

To characterise the transformation U_1 across all input spatial and polarisation modes, we change the multi-photon source to a laser source ($\lambda = 1550 \pm 3nm$) that maintains the paths shown in S.1 for s_1, s_2 . We then allow the light from s_i to be injected into the MMF, one by one for $i = 1, 2$ while random patterns x_{1_i}, x_{2_i} are displayed on SLM₁ and SLM₂ respectively. The modulated light at the output is measured on the camera. We employ a multi-plane neural

network (MPNN) [26] to learn the transmission matrix of the MMF for each input polarization U_{1_i} by optimizing the following cost function

$$\min_{U_{1_i}} |y_i - |U_2(x_2 \odot (U_{1_i} x_{1_i}))|^2| \quad (\text{S.2.1})$$

Stacking the transmission matrices from each polarization U_{1_i} allows us to construct U_1 . This method enables us to bypass the need for an external reference with a machine-learning model that describes the optical system of the experiments.

Since the transmission matrices U_{1_i} are measured independently, we have no information on the relative phase between different input polarisations. While this phase doesn't affect the performance of the circuit when routing or switching entanglement, the effect on the entanglement swapping protocol is to introduce a phase on the state between Ada and Hedy of the form $|\Psi\rangle = (|01\rangle + e^{i\varphi}|10\rangle)$.

To make sure the classical characterisation of the spatial mode-mixing process inside the fibre reproduces the behaviour of the SPDC photons, we use a system of telescopes for careful mode-matching between the laser source and the estimated spatial distribution of the multimodal SPDC emission [35]. To characterise the coupling loss in the circuit, we measure the coupling efficiency from the free-space single-mode laser source to the MMF to be above 76%.

With the complete knowledge of the scattering processes in the mode-mixer, target circuits can be inverse-designed using phase pattern solutions for planes P_1, P_2, P_3 and P_4 that are calculated with iterative wavefront matching (WFM) optimisations of input and output optical fields [25]. For this, input and output modes are generated for a chosen set of discrete spatial mode bases and target transformation \mathbb{T} . Each of the input modes is computationally forward propagated, while each output mode is backwards propagated to each of the phase layers comprising of phase planes $\{P_1, P_2\}$ and $\{P_3, P_4\}$. The phase of each of these planes is then updated to minimize the phase difference between the wavefront of input and output modes. This process is repeated a few times until a convergence is observed. We then display the optimised phase-plane solutions P_1, P_2, P_3 and P_4 in the physical setup for it to work as an optical circuit.

S.3. Programmable routing of entanglement over a single channel

To route d -dimensional entanglement (with $d = 2, 3$) using a single channel between pairs of users, we start by considering the truncated input entangled states of the form $|\Phi\rangle = \frac{1}{\sqrt{d}} \sum_{i=0}^{d-1} |ii\rangle$. The set $\{|d\rangle\}_d$ forms a d -dimensional macro-pixel basis. On the input side of the circuit, we select the macro-pixel modes $\{|0\rangle_1, \dots, |d\rangle_1, |0\rangle_2, \dots, |d\rangle_2\}$, where the subscripts 1 and 2 indicate which input signal photon the modes correspond to. For the output modes, we select d foci on each of the output ports of the circuit, which are directed to B and G. On A and H, single-outcome projective measurements on the d -dimensional macro-pixel basis over the idler photons herald the corresponding input modes.

The simultaneous distribution of two-dimensional entanglement between AB and GH (AG and BH) is achieved with the 4x4 dimensional \mathbb{I} (\mathbb{X}) gate. We can also program 6x6 dimensional \mathbb{I} (\mathbb{X}) operations to share three-dimensional entanglement between AB and GH, or AG and BH.

As described in II, we use two-fold coincidence measurements in all mutually unbiased bases (Fig. S.2) to estimate fidelities to the maximally entangled state in dimensions $d = 2, 3$ [30]. As shown in Table S.2, the obtained fidelities violate the dimensionality bounds with several standard deviations, allowing us to certify the routing of two-dimensional and three-dimensional entanglement over the network.

S.4. Circuit stability

We study the stability of the complex media-based circuit by characterising the performance of the programmable circuit over time. With a single initial characterisation of the mode-mixing in the MMF, and without performing any experimental realignment, we regularly test our highest-dimensional gates (8×8) over 14 days. Fidelity estimates of the states shared over the two channels are obtained through two-fold coincidence measurements on all mutually unbiased basis. As shown in Fig. S.3, the resulting fidelities, calculated with one standard deviation, consistently exceed the bound for a two-dimensional separable state. The consistent certification of the multiplexed and adaptable entanglement routing over time demonstrates the robustness of our platform.

Table S.2: Fidelities to the maximally entangled state of the states shared in the programmable network using a single channel

Gate	2-dim states		3-dim states	
	AB	GH	AB	GH
\mathbb{I}	$86.2 \pm 1.1\%$	$83.1 \pm 1.1\%$	$73.1 \pm 1.8\%$	$77.0 \pm 1.5\%$
\mathbb{X}	AG	BH	AG	BH
	$81.2 \pm 1.2\%$	$83.6 \pm 1.2\%$	$77.4 \pm 1.8\%$	$74.7 \pm 1.8\%$
SWAP	AH		-	
	88.1 ± 2.0		-	

*Errors are reported to three standard deviations

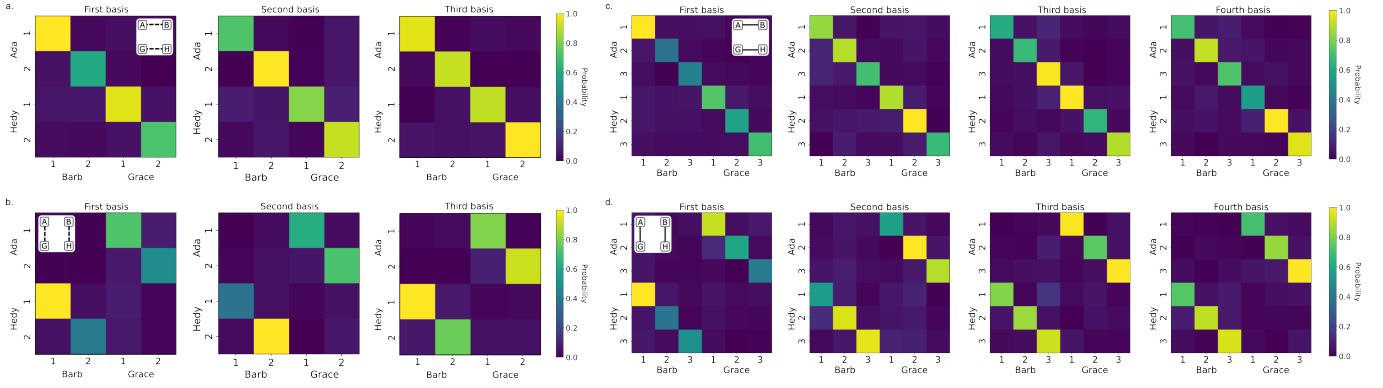


Figure S.2. Two-dimensional and three-dimensional entanglement routing. We distribute entanglement between two users via a single channel either with a two-dimensional entangled state (a,b) or a three-dimensional state (c,d). We perform measurements on mutually unbiased bases to characterise the operation of each configuration. The correlation matrices correspond to two-fold coincidence measurements on the first (left) and second (right) bases, showcasing the circuit's operation.

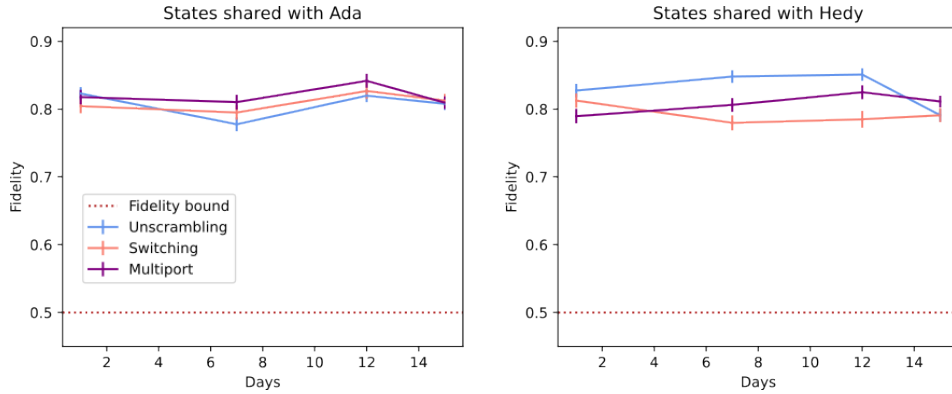


Figure S.3. Entanglement routing stability. We measure the fidelities to the 2-dimensional maximally entangled state of the states shared with the three different 8×8 unitary gates, implemented repeatedly over two weeks. Average fidelities over the two channels and pairs of parties are estimated with each gate. With \mathbb{T}_I , entanglement is either routed between AB and GH (Unscrambling), between AG and BH (Switching) with \mathbb{T}_S , or distributed from one party to the other two separate parties with \mathbb{T}_M (Multiport). The red dotted line indicates the fidelity bound for a separable state.

S.5. Entanglement swapping

An initial basic operation is to swap entanglement over one single channel per party. We consider two-dimensional input states of the form: $|\phi\rangle = \frac{1}{\sqrt{2}}(|00\rangle + |11\rangle)$, each produced by a different source. The complete initial four-photon state is then described as

$$|\Phi\rangle = \frac{1}{2}(|0000\rangle + |0101\rangle + |1010\rangle + |1111\rangle), \quad (\text{S.5.1})$$

where each element of the ket corresponds to the state of the photons s_1, s_2, i_1, i_2 .

The entanglement swapping operation acting on signal photons s_1 and s_2 of $|\Phi\rangle$ is defined by the operation:

$$\mathbb{T}_S = \frac{1}{\sqrt{2}} \begin{bmatrix} 1 & 0 & 1 & 0 \\ 0 & 1 & 0 & 1 \\ 1 & 0 & -1 & 0 \\ 0 & 1 & 0 & -1 \end{bmatrix} \quad (\text{S.5.2})$$

Following the transformation, we perform four-fold coincidence measurements between the output ports and the heralding photons, projecting the state shared between the parties Ada and Hedy onto the maximally entangled target state $|\Psi\rangle = (|01\rangle + e^{i\varphi}|10\rangle)$, where φ is a relative phase between the two sources introduced by the set-up.

This single-channel entanglement swapping protocol can be extended to operate across two simultaneous channels. In this scenario, the state of each source is expressed as $|\phi\rangle = \frac{1}{\sqrt{2}}(|\phi\rangle^{(\text{chI})} + |\phi\rangle^{(\text{chII})})$, where $|\phi\rangle^{(\text{chI})} = \frac{1}{\sqrt{2}}(|00\rangle + |11\rangle)$ and $|\phi\rangle^{(\text{chII})} = \frac{1}{\sqrt{2}}(|22\rangle + |33\rangle)$. Consequently, the initial four-photon state becomes a four-dimensional entangled state of the form:

$$|\Phi\rangle = \frac{1}{2} \left(|\phi\rangle_1^{(\text{chI})} + |\phi\rangle_1^{(\text{chII})} \right) \otimes \left(|\phi\rangle_2^{(\text{chI})} + |\phi\rangle_2^{(\text{chII})} \right) \quad (\text{S.5.3})$$

where the subscript indicates the source. Then, the unitary operation that allows us to swap entanglement is given by Eq. 1 in the main text.

After the transformation of the signal photon states, we measure four-fold coincidences at each output over each channel, projecting the states shared between Ada and Hedy onto two different maximally entangled target states: $|\Psi\rangle^{(\text{chI})} = \frac{1}{\sqrt{2}}(|01\rangle - e^{i\varphi}|10\rangle)$ and $|\Psi\rangle^{(\text{chII})} = \frac{1}{\sqrt{2}}(|23\rangle - e^{i\varphi}|32\rangle)$. As before, φ represents the relative phase introduced by the setup. This process allows us to obtain two distinct swapped states between Ada and Hedy at the same time.

In both cases, by applying a quantum state tomography detailed in S.6, we determine the relative phase and reconstruct the estimated states for each scenario and channel, achieving fidelities to the target state $|\Psi\rangle$ of more than 77%, thus successfully validating our protocol.

S.6. Quantum State Tomography

Each realisation of the SWAP gate in the programmable quantum network generates a bipartite quantum state between Ada and Hedy upon which we perform full quantum state tomography by measuring a tomographically complete set of measurements consisting of all local Pauli eigenvectors and performing Maximum-likelihood state estimation [42]. The complete set of measurements consists $\{\Pi_{ambn}^{AH} = \Pi_{a|m}^A \otimes \Pi_{b|n}^H\}_{ambn}$ where $\Pi_{a|m}^A = |v_{a|m}\rangle\langle v_{a|m}|$ and $a \in \{1, -1\}$ indexes the eigenvector of the Pauli matrix, σ_m for $m \in \{X, Y, Z\}$. For each measurement, n_{ambn} 4-photon coincidences are recorded and the maximum-likelihood estimator is obtained by iterating,

$$\rho_{k+1} = \mathcal{N}[\mathcal{R}(\rho_k)\rho_k\mathcal{R}(\rho_k)], \quad (\text{S.6.1})$$

where

$$\mathcal{R}(\rho) := \sum_{i \sim ambn} \frac{1}{M_{mn}} \frac{n_i}{\text{Tr}[\Pi_i^{AH}\rho]} \Pi_i^{AH}, \quad (\text{S.6.2})$$

with $\rho_0 = \mathbb{I}/d$ taken as the maximally mixed state, $M_{mn} = \sum_{ab} n_{ambn}$ is the 4-photon events in each basis, and $\mathcal{N}[\rho] := \rho \text{Tr}[\rho]$ imposes unit trace. To estimate the statistical noise present in our state estimates we perform Monte-Carlo bootstrapping by taking Poissonian samples from our data and repeating the estimation procedure. We obtain 2000 state estimates and their corresponding state fidelities to arrive at the 1STD standard error stated on our presented state fidelities.

We perform quantum state tomography to recover the density matrix of the state shared by A and H to demonstrate the success of our entanglement swapping protocol. We estimate a fidelity to the two-dimensional maximally entangled target state of $88.1 \pm 2.0\%$ for single channel swapping. In the multiplexed case, we estimate fidelities of $77.1 \pm 3.3\%$ for the first channel and $83.2 \pm 2.7\%$ for the second channel.